ACS APPLIED MATERIALS & INTERFACES

Research Article

www.acsami.org

High-Performance Inverted Tandem Polymer Solar Cells Utilizing Thieno[3,4-*c*]pyrrole-4,6-dione Copolymer

Abd. Rashid bin Mohd Yusoff,[†] Seung Joo Lee,[†] Jaeyeon Kim,[†] Fabio Kurt Shneider,[‡] Wilson Jose da Silva,[‡] and Jin Jang*,[†]

[†]Department of Information, Display and Advanced Display Research Center, Kyung Hee University, Dongdaemun-ku, Seoul 130-171, Republic of Korea

[‡]Universidade Tecnologica Federal do Parana, GPGEI−Avenida Sete de Setembro, 3165−CEP 80230-901−Curitiba, Parana Brasil

Supporting Information

ABSTRACT: We demonstrated the inverted solution processed tandem polymer solar cells, in which transparent pH-neutral poly(3,4-ethylenedioxylenethiophene)−polystylene sulfonic acid (PEDOT:PSS) and lithium zinc oxide layers were used as a recombination layer. We have used poly(di(2-ethylhexyloxy)-benzo[1,2-*b*:4,5-*b*′]dithiophene-*co*-octylthieno[3,4-*c*]pyrrole-4,6-dione):[6,6]-phenyl-C_{61} butyric acid methyl ester (PBDTTPD:$PC_{61}BM$) and poly[(4,4′-bis(2-ethylhexyl)dithieno[3,2-*b*:2′,3′-*d*] silole)-2,6-diyl-*alt*-(2,1,3-benzothiadiazole)-4,7-diyl]:[6,6]-phenyl-C_{70} butyric acid methyl ester (PSBTBT:$PC_{70}BM$) as the active layers for front and rear subcells, respectively. The pH-neutral PEDOT:PSS/LZO serves as an electron- and hole-collecting and recombination layer. Our tandem solar cells showed a high open circuit voltage (V_{oc}) of 1.54 V, a short circuit current density (J_{sc}) of 7.55 mA/cm^2, and a fill factor (FF) of 64.79% along with the power conversion efficiency of 7.53%. The V_{oc} value of our tandem solar cells is an ideal summation of V_{oc} values from front and rear subcells.

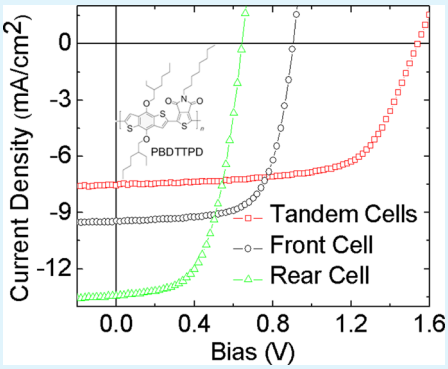

KEYWORDS: *tandem structure, polymer solar cells, recombination layer, pH-neutral PEDOT:PSS, metal oxide, solution processed*

1. INTRODUCTION

Recently, there have been remarkable advances in photovoltaic technology, especially in multiple-junction photovoltaic devices, where two or more single-junction photovoltaic devices are stacked to achieve higher solar absorption.[1−10] A multiple junction photovoltaic device, also known as a tandem cell, offers various advantages over single-junction solar cells. When single-junction cells are connected in series, it provides significantly higher open circuit voltage (V_{oc}), while if they are connected in parallel, they could obtain higher short circuit current density (J_{sc}). Today, there are many types of tandem cells such as small molecules,[11,12] dye-sensitized,[13−15] inorganic,[16−18] and hybrid,[19−23] as well as polymer[24−27] tandem cells.

In late 2012, Heliatek,[28] one of a leading research entities working on small molecules tandem cells, announced that they achieved 12% power conversion efficiency (PCE) along with an impressive V_{oc} of 2.19 V. Not long after, Yang et al.[29] reported a 10.6% PCE using a band gap material provided by Sumitomo Chemical. Later in 2013, Janssen et al.[30] published a decent work on triple tandem cells which gives 9.2% PCE. Recently, Yusoff et al.[31] have reported that 8.91% tandem cells incorporating a highly promising polymer, poly[(4,4′-bis(3-ethylhexyl)dithieno[3,2-*b*′′:3′-*d*]silole)-2,6-diyl-*alt*-(2,5-(3-(2-ethylhexyl)thiophen-2-yl)thiazolo[5,4-*d*]thiazole] (PSEHTT).

Apart from high efficiency tandem cells, a primary challenge when fabricating tandem cells is finding an ideal interconnecting layer (ICL) that not only connects, but also physically separates the front and rear subcells. Previously, researchers have proposed using transparent conductive oxide for the ICL due to its low sheet resistance and high optical transparencies in the visible region, which is beneficial also for photon transmission. However, these materials are usually deposited by means of a sputtering process, which can cause plasma damage to the underlying organic cell, making it less appealing.[32−34] On the basis of the aforementioned issues, it is pretty undesirable to fabricate high efficiency tandem cells using a sputtering process.

Despite recent advances in photovoltaic technology, especially tandem cells, reports on high-performance tandem cells using the inverted architecture remain limited. The essential challenge lies in designing and constructing the ideal combination zone of two subcells, the ICL. While complementary absorptions of the tandem structure meets this optical prerequisite, the ICL inserted between the front and rear subcells should not only be robust enough to protect the underlying layers against subsequent layer depositions but also

Received: May 14, 2014
Accepted: June 26, 2014
Published: June 26, 2014

provide effective electrical contact. Fundamentally, the ICL functions as a zone that brings together the electron quasi-Fermi level of one subcell and the hole quasi-Fermi level of the other, adding up the potential of the two polymer bulk heterojunctions (BHJs). Therefore, the ICL simultaneously satisfies the prerequisites for a high-performance tandem cell in optical and electrical properties.

We investigate the tandem cell utilizing inverted architecture, incorporating a stack of polymeric and metal oxide ICL to electrically connect two donor−acceptor BHJs that cover a wide range of complementary absorption. In our inverted tandem cell, the front and rear subcells were separated by a transparent pH-neutral poly(3,4-ethylenedioxylenethiophene)−polystylene sulfonic acid (PEDOT:PSS) and lithium zinc oxide (LZO) layer. The pH-neutral PEDOT:PSS, acting as hole-transport layer (electron blocking layer), was deposited using a spin-coating technique. Because of its high transparency, the light intensity reaching the rear subcell is high, resulting in increased photocurrent. LZO was used as the electron transport layer (hole-blocking layer) with holes from the front subcell combined with electrons from the rear subcell at the pH-neutral PEDOT:PSS/LZO ICL. The molecular structures of poly(di(2-ethylhexyloxy)benzo[1,2-*b*:4,5-*b*′]dithiophene-*co*-octylthieno-[3,4-*c*]pyrrole-4,6-dione) (PDBTTPD)[35] and poly[(4,4′-bis(2-ethylhexyl)dithieno[3,2-*b*:2′,3′-*d*]silole)-2,6-diyl-*alt*-(2,1,3-benzothiadiazole)-4,7-diyl] (PSBTBT),[25] the tandem cell structure, and the energy band diagram of the proposed inverted tandem cell are shown in Figure 1. We carefully designed an inverted

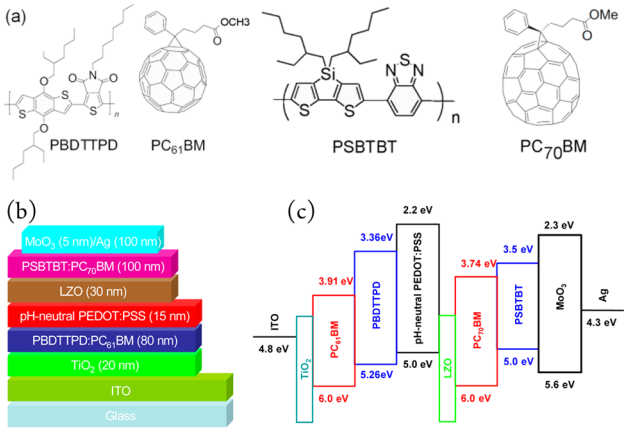

Figure 1. (a) Chemical structures of the polymers (PBDTTPD and PSBTBT) and fullerene ($PC_{61}BM$ and $PC_{70}BM$) used in polymer tandem solar cells. (b) Tandem device structures: glass/ITO/TiO_2/PBDTTPD:$PC_{61}BM$/pH-neutral PEDOT:PSS/LZO/PSBTBT:$PC_{70}BM$/MoO_3/Ag. (c) Energy diagram of the polymer tandem solar cells.

tandem cell using pH-neutral PEDOT:PSS/LZO ICL to yield 7.53% PCE. Our results illustrate that an ideally connected front and rear subcells can be established by this polymeric stacked metal oxide ICL. In this study, 173 tandem cells were made, with the best device PCE of 7.53%. In the course of this study, we fabricated 147 tandem cells with PCEs greater than 7%. It is worth noting that our device performance is not as good as previously published works; however, our proposed interconnecting layer can be considered among the best, since the V_{oc} for tandem cell is an exact summation of the V_{oc}'s of the front and rear subcells.

2. RESULTS AND DISCUSSION

To create a high-performance tandem cell, we carried out extensive optimization to determine the optimal thicknesses for the front and rear subcells. Since the two subcells are electrically connected in series, the photocurrent of the tandem cell is limited by the lowest photocurrent of either front or rear subcells. Therefore, the photocurrents of the top and bottom subcells must be balanced in order to optimize the performance of the tandem cell. This is primarily accomplished through control of active layer thickness and proper choice of BHJ blends possessing different optical band gaps in each subcell. To establish the right thickness of the BHJ layers in the inverted tandem cell, separated single-junction solar cells ITO/TiO_2/PBDTTPD:$PC_{61}BM$/HTL/Al and ITO/ETL/PSBTBT:$PC_{70}BM$/MoO_3/Ag were prepared with a range of active layer thicknesses. For each layer thickness, we characterized the cells and then determined the spectrally averaged internal quantum efficiency (IQE) based on the ratio between the short-circuit current (obtained by integrating the product of the solar spectrum with the experimental EQE of the solar cell) and the absorbed flux of photons from the standard global air mass 1.5 sunlight (AM1.5G).

First, we performed solvent resistance treatments analysis of pH-neutral PEDOT:PSS/LZO for various different solvents (chlorobenzene, dichlorobenzene, trichlorobenze, and chloroform) as well as LZO thin film characterizations, including transmittance, refractive index, extinction coefficient, resistivity, and Hall mobility. On the other hand, Figure S1 (Supporting Information) demonstrates the transmittance of LZO layer as a function of wavelength along with *n* and *k* values. From Figure S1b (Supporting Information), the refractive index decreases with the increasing wavelength (400−800 nm). Figure S1c (Supporting Information) shows the extinction coefficient of the LZO as a function of wavelength. It can be seen that the extinction coefficient also decreases with the increment of wavelength. Finally, Table S1 (Supporting Information) collects the resistivity and Hall mobility values at different lithium concentration in LZO. On the basis of the above-mentioned characteristics, including its high Hall mobility and transparency, we have selected LZO as ICL instead of ZnO.

Figure 2a shows the optical simulation optimization studies on thermal annealing effects of PBDTTPD:$PC_{61}BM$. In this simulation, we used the physical parameters for various annealing temperatures. This contour plot reveals that an annealing process between ∼105 and 115 °C gives the best J_{sc} output. Thus, on the basis of this simulation, we designed a comprehensive study of our front subcell single-junction devices. The first experimental optimization experiments of the front subcell are based on PBDTTPD:$PC_{61}BM$ BHJ with different thicknesses from 70 to 90 nm as well with different HTLs under 100 mW/cm^2 AM1.5G illumination. Figure 2b shows the *J*−*V* characteristics of the BHJ solar cells with various thicknesses of BHJ layer. The PCE critically depends on the thickness of the BHJ layer. The PCEs of the BHJ solar cells are 5.21, 5.77, and 5.10% for the cells with 70, 80, and 90 nm BHJ, respectively. There is also an increase in the FF from 63.20% for the cell with thinner BHJ (70 nm) to 67.77% for the cell with slightly thicker BHJ (80 nm). However, the FF decreases when the thickness of BHJ increases to 100 nm, leading to a decrease in the PCE. From the *J*−*V* characteristics, we observed that an 80 nm thick BHJ layer reduces the series resistance (R_s) and increases the shunt resistance (R_{sh}), leading to improved

dx.doi.org/10.1021/am5029318 | ACS Appl. Mater. Interfaces 2014, 6, 13079−13087

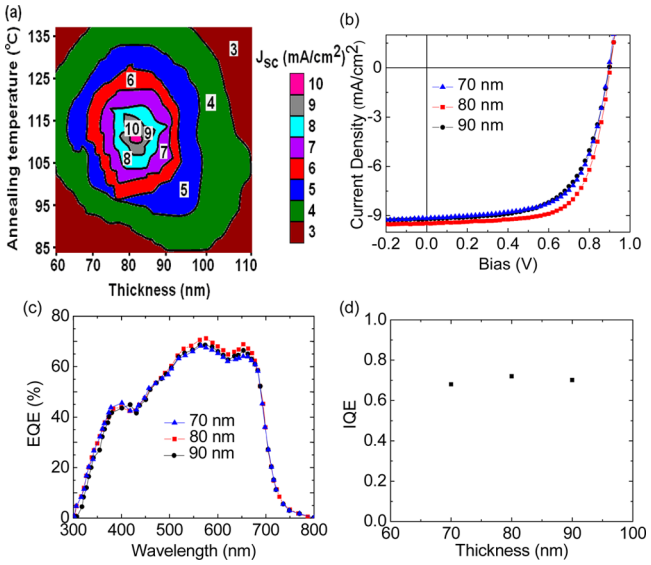

Figure 2. PBDTTPD:PC61BM-based single-junction solar cells performance with different active layer thicknesses under simulated AM1.5G illumination at 100 mW/cm^2. (a) Optical simulation of annealing temperature vs thickness of active layer. (b) $J-V$ curves. (c) External quantum efficiency. (d) Internal quantum efficiency.

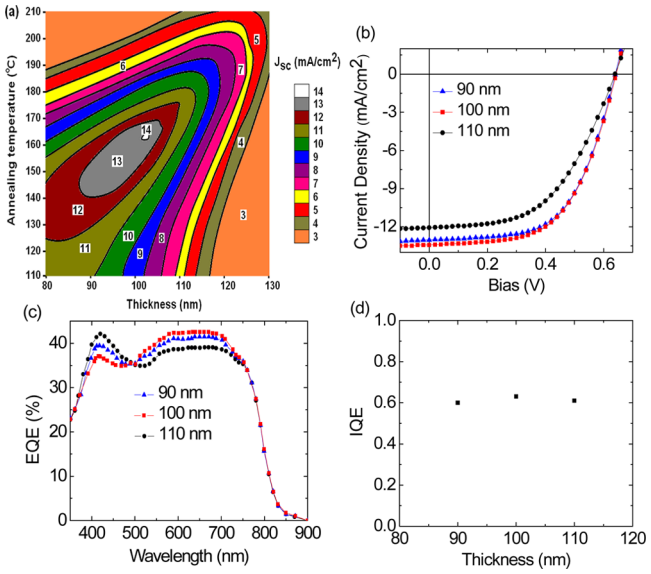

Figure 3. PSBTBT:PC_{70}BM-based single-junction solar cells performance with different active layer thicknesses under simulated AM1.5G illumination at 100 mW/cm^2. (a) Optical simulation of annealing temperature vs active layer thickness. (b) $J-V$ curves. (c) External quantum efficiency. (d) Internal quantum efficiency.

FF and J_{sc}. In addition, the device with a moderate BHJ layer (80 nm) shows an excellent diode quality factor of 1.5 in the dark $J-V$ characteristics with very low leakage current. The detailed photovoltaic parameters of the cells with various thicknesses of BHJs are tabulated in Table 1. Table S2 (Supporting Information) includes the R_s and R_{sh} resistances for all fabricated single-junction PBDTTPD:PC_{61}BM-based devices. Figure 2c shows the EQE spectra of the device with different BHJ thicknesses. The EQE value exceeds 65% over the wavelength range between 560 and 590 nm for a device with 80 nm BHJ. To fully characterize the performance of the cells, we also measured the IQE of the PBDTTPD:PC_{61}BM BHJ solar cells, as shown in Figure 2d. The IQE is the ratio of the number of the charge carrier collected by the solar cell to the number of photons of given energy that is absorbed by the cell. After measuring the total absorption in the cell through normal incidence reflectance methods, the mean spectral averaged 40% with a standard deviation of 2%. It is worth noting that the IQE value is less than 80%. This indicates that not every absorbed photon is converted to separate charges in the donor and acceptor domains and that these photogenerated charge carriers are collected at the electrodes.

Optical simulation of thermal annealing is again conducted to find the best annealing temperature for PSBTBT:PC_{70}BM (Figure 3a). Figure 3a demonstrates that an annealing temperature of ~160 °C leads to approximately J_{sc} ~ 14 mA/cm^2. As the temperature gets higher, the J_{sc} becomes lower. Second, experimental optimization has been performed on ITO/ETL/PSBTBT:PC_{70}BM/MoO_3/Ag with different BHJ thicknesses under 100 mW/cm^2 AM1.5G illumination. Figure 3b demonstrates that $J-V$ curves depend on the thickness of the BHJ layer. The V_{oc} is not strongly dependent on BHJ layer thickness, where the V_{oc}'s of 0.64 V can be obtained within the range of BHJ layer thicknesses of 90−110 nm. The J_{sc} increases from 13.04 to 13.44 mA/cm^2 as the BHJ layer thickness increases to 100 nm and reduces to around 12.07 mA/cm^2 when the BHJ layer is greater than 100 nm (see Table 2). Table S3 (Supporting Information) shows the R_s and R_{sh} for all fabricated single-junction PSBTBT:PC_{70}BM-based devices. Due to the diminishing FF and J_{sc}, PCE clearly decreases with the increase of the BHJ layer thickness. The film of 90 nm can deliver a PCE of 4.9% and can achieve 4.94% from 100 nm. The ideality factor was found to be independent of the BHJ layer thickness. To obtain information on the contribution of incident photons of the photocurrent, EQE measurements were conducted on single-junction solar cells having different BHJ layer thicknesses. EQE spectra showed similar behavior with the absorption spectra of PSBTBT, indicating that absorption wavelengths between 350 and 900 nm are all contributing to the photocurrent. The EQE curves reached a broad maximum at 450 nm, remaining at a level of 48% up to 750 nm (Figure 3c). The highest value found was 42% when the same was 100 nm in BHJ layer thickness, which was also the one with the highest PCE.[26] The EQE results are in good accordance with

Table 1. Device Performance of PBDTTPD:PC_{61}BM-Based Inverted Single Junction Solar Cells with Different Active Thicknesses and Different Hole Transport Layers

active layer thickness (nm)	HTL	J_{sc} (mA/cm^2)	V_{oc} (V)	FF (%)	PCE (%)
80	WO_3	8.02 ± 0.2	0.90 ± 0.01	63.59 ± 0.02	4.59 ± 0.12
70	PEDOT:PSS	9.17 ± 0.1	0.90 ± 0.01	63.20 ± 0.01	5.21 ± 0.10
80	PEDOT:PSS	9.46 ± 0.01	0.90 ± 0.01	67.77 ± 0.14	5.77 ± 0.15
90	PEDOT:PSS	9.22 ± 0.3	0.90 ± 0.01	61.46 ± 0.11	5.10 ± 0.02
80	V_2O_5	8.74 ± 0.1	0.90	63.02	4.96 ± 0.21

dx.doi.org/10.1021/am5029318 | ACS Appl. Mater. Interfaces 2014, 6, 13079−13087

Table 2. Device Performance of PSBTBT:$PC_{70}BM$-Based Inverted Single-Junction Solar Cells with Different Active Thicknesses and Different Electron Transport Layers

active layer thickness (nm)	ETL	J_{sc} (mA/cm^2)	V_{oc} (V)	FF (%)	PCE (%)
80	TiO_x	12.85 ± 0.1	0.64 ± 0.01	56.34 ± 0.11	4.63 ± 0.10
80	LZO	12.52 ± 0.1	0.64 ± 0.01	52.11 ± 0.10	4.21 ± 0.06
90	LZO	13.04 ± 0.2	0.64 ± 0.01	58.68 ± 0.11	4.90 ± 0.12
100	LZO	13.44 ± 0.1	0.64 ± 0.01	57.50 ± 0.08	4.94 ± 0.10
110	LZO	12.07 ± 0.2	0.64 ± 0.01	51.76 ± 0.14	3.99 ± 0.10
80	AZO	11.64 ± 0.1	0.64 ± 0.01	42.54 ± 0.10	3.69 ± 0.14

the J_{sc} values. It is worth noting that if the calculated J_{sc} from EQE spectra is not in a good agreement with the J_{sc} obtained from the $J-V$ characteristics, it indicates that the measured I_{sc} is overestimated. The appearance of an EQE curve plateau indicates that cells harvest efficiently the incident photons, converting them with a high quantum yield to electric current. The electrical losses at various BHJ layer thicknesses are independent of device absorption and attributed to the exciton and carrier behavior inside the device. The spectrally averaged IQE was 60%, with a standard deviation of 2%. The variations in IQE with layer thickness are less than the experimental error (Figure 3d).

In this study, our tandem cell consists of wide band gap BHJ (PBDTTPD:$PC_{61}BM$) stacked with small band gap BHJ (PSBTBT:$PC_{70}BM$). These polymers provide rather efficient single-junction cells,[35,36] exhibiting V_{oc}'s of about 0.9 and 0.64 V, respectively. A stack of pH-neutral PEDOT:PSS and solution-processed LZO is used as recombination layer.

Figure 4a shows the simulation data as a function of different thicknesses for the front and rear subcells. One could achieve a maximum efficiency of 8% with suitable front and rear subcells thicknesses.

Figure 4b shows the $J-V$ characteristics of front, rear, and tandem solar cells under AM1.5 simulated illumination with the intensity of 100 mW/cm^2. The solar cell parameters are summarized in Table 3. Table S4 (Supporting Information) tabulates the R_s and R_{sh} for front and rear subcells and a tandem cell. The front (PBDTTPD:$PC_{61}BM$) single solar cell exhibits a V_{oc} of 0.90 V, a J_{sc} of 9.46 mA/cm^2, a fill factor (FF) of 67.77%, and a PCE of 5.77%. The rear (PSBTBT:$PC_{70}BM$) single solar cell exhibits a V_{oc} of 0.64 V, a J_{sc} of 13.44 mA/cm^2, a FF of 57.50%, and a PCE of 4.94%. The tandem solar cell yields a V_{oc} of 1.54 V, J_{sc} of 7.55 mA/cm^2, a FF of 64.79%, and a PCE of 7.53%. The V_{oc} of the tandem solar cell is 1.54 V, reaching 100% of the summation of the subcells V_{oc} values. This provides evidence that the front and rear subcells were successful and efficiently connected in series. Furthermore, it also proves that pH-neutral PEDOT:PSS/LZO serves as a perfect ICL. In order to get a better understanding of the proposed ICL, ultraviolet photoelectron spectroscopy (UPS) was used to determine and understand the origin of the difference in device performance, specifically the role of the ICL.[37] A detailed description is found elsewhere; however, in brief, due to the fact that the V_{oc} of our tandem cell is the ideal summation of the V_{oc}'s from the front and rear subcells, there is a perfect quasi-Fermi level alignment between hole and electron coming from the front and rear subcells, respectively. A p−n junction is formed between pH-neutral PEDOT:PSS and LZO with a negligible offset between the LUMO of pH-neutral PEDOT:PSS and the HOMO of LZO. This negligible offset between the LUMO of pH-neutral PEDOT:PSS and the HOMO of LZO diminishes energy loss when the generated hole from the front subcell and electron from the rear subcell recombine in the ICL. Therefore, the charge conduction and recombination processes easily take place along with a neglected voltage drop, and consequently, the obtained V_{oc} in our tandem cell (1.54 V) is the ideal summation of the V_{oc}'s for the front and rear subcells.

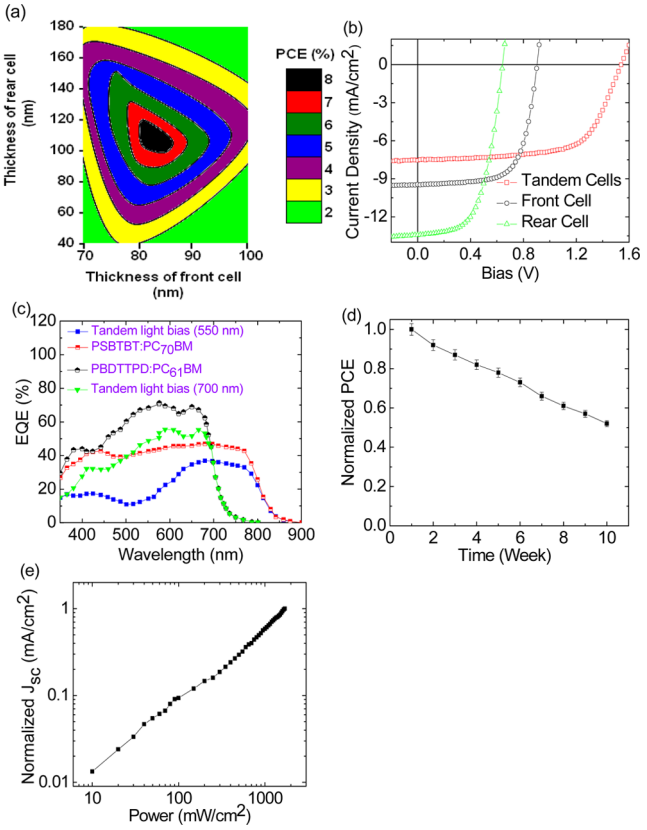

Figure 4. (a) Simulated photocurrent generated in tandem cells as a function of the thickness of the front and rear active layers. (b) $J-V$ curves of front, rear, and tandem cells under simulated AM1.5G illumination at 100 mW/cm^2. (c) EQE measured under relevant bias illumination conditions and correct electrical bias. (d) Stability of the tandem cells over 60 days. (e) Normalized (to the value obtained at 1700 mW/cm^2) J_{sc} of tandem cell as a function of illumination intensity. A tandem cell shows linear dependence on illumination intensity up to 1700 mW/cm^2.

Table 3. Device Performance of Front, Rear, And Tandem Cells

structure	J_{sc} (mA/cm^2)	V_{oc} (V)	FF (%)	PCE (%)
front	9.46 ± 0.01	0.90 ± 0.01	67.77 ± 0.14	5.77 ± 0.15
rear	13.44 ± 0.1	0.64 ± 0.01	57.50 ± 0.08	4.94 ± 0.10
tandem	7.55 ± 0.03	1.54 ± 0.01	64.79 ± 0.03	7.53 ± 0.02

Moreover, when we introduced another concept of ICLs,[37] these ICLs combined to give a large energy offset, resulting in large built-in potential across the interface and, consequently, a limit on the recombination process. Hence, the tandem cell with other proposed ICLs experience major loss in V_{oc} compared to the tandem cell utilizing pH-neutral PEDOT:PSS/LZO ICL.[37] The J_{sc} of the tandem cell is about 7.55 mA/cm^2, approaching the J_{sc} of the single cells (J_{sc} = 9.46 mA/cm^2 for front subcell and J_{sc} = 13.44 mA/cm^2 for rear subcell), which results in only partially overlapped absorption of the PBDTTPD:PC_{61}BM and PSBTBT:PC_{70}BM films at the visible regime and the optical field redistribution in tandem architecture when both front and rear subcells were stacked.

As one can see, the J_{sc} of the rear subcell, which has a thicker BHJ layer, is not saturated. The increase in photocurrent at reverse bias (date not shown) is caused by an increased absorption of the BHJ layer and field-dependent photogeneration efficiency. There is a slight increase in PCE (from 4.90 to 4.94%) because the J_{sc} in the rear subcell increases to 13.4 mA/cm^2, although there is a small decrease in FF from 58.68 to 57.50%.

In addition, a high FF of 64.79% (tandem cell) is retained, indicating that the photogeneration in the tandem subcells is relatively field-independent. A high FF in the tandem cell is achieved because of (i) efficient carrier transport, (ii) the efficient charge carrier recombination at the designed interlayer, and (iii) a redistribution of the built-in electric field in the subcells as a result of the required current matching in the subcells.[38] Furthermore, high FF also indicates that the proposed ICL (pH-neutral PEDOT:PSS/LZO) served as an ideal junction for both electrons and holes from rear and front subcells, respectively.

Finally, the gain in V_{oc} (tandem cell), which is more than offset by the reduction of J_{sc}, forms the PCE value of the tandem cell as 7.53%, which is higher than that of either of the two subcells individually (5.77% and 4.94%, respectively).

The two single-junction solar cells are electronically linked together by the pH-neutral PEDOT:PSS/LZO ICL (Figure S2, Supporting Information). Figure S2 (Supporting Information) shows the ICL that successfully separated the front and rear subcells. Since the front and rear subcells are connected in series, this ICL provides a recombination zone of holes and electrons approaching from the front and rear subcells, respectively. In order to efficiently extract the holes from the front subcell and the electrons from the rear subcells, the ICL needs to provide a quasi-Ohmic contact. Otherwise, insufficient recombination will result in limited currents in both devices. The ICL has to act as the anode (with a high work function to align with the HOMO of the donor) for the front subcell and, at the same time, as the cathode (with a low work function to align with the LUMO of the acceptor) for the rear subcell. Finally, the ICL must be as thin as possible to minimize optical losses.

Figure 4c shows the EQE of each subcell with the tandem cell device alongside the absorptance spectra of the corresponding BHJ layers. Special attention must be given during EQE measurements of the tandem solar cell because of the coupled light absorption and current-generation processes in the front and rear subcell.[8] Thus, in order to precisely acquire the EQE spectra, EQE measurements were gathered with two excitation light sources, (i) a 700 nm light optical bias light beam to excite only one of the subcells and (ii) a 550 nm light to measure the EQE of the other subcell. The EQE spectra demonstrates an excellent match in photocurrent generated by the front and rear subcells. The EQE spectra of the front and rear subcells strongly follow its absorptance spectra, indicating that the photocurrents are generated from the PBDTTPD:PC_{61}BM and PSBTBT:PC_{70}BM BHJ layers.

As PCE has recently increased, another important consideration in tandem cell lies in their stability and longevity. Despite being fully encapsulated, the efficiency of single-junction solar cell usually deteriorates 25−30% under continuous illumination (4000 h).[39] Figure 4d shows a shelf-life test in air of our tandem cell. The tandem cell with original efficiency of 7.5% survived for the 5 weeks degradation test, where the efficiency drops by 22%. However, after 10 weeks of continuous illumination, the efficiency drops to 3.92%. It is known that inverted cells usually have better air stability compared to their counterpart. These observations indicate that although encapsulation can be considered as one alternative to alleviate any degradation process, in order to fully understand the real degradation mechanism as well as to further enhance the shelf-life of one particular cell, detailed and comprehensive works are needed.

The normalized J_{sc} of the tandem cell with optimized ICL shows a linear dependence on the illumination intensity for the tandem cell, as depicted in Figure 4e. The J_{sc} was normalized to that obtained under 1700 mW/cm^2. Although executed at higher light intensities (~1700 mW/cm^2), there is no clear evidence to support that substantial space charge built up in the tandem cell would cause enhanced carrier recombination and sublinear dependence of J_{sc} on illumination intensity.

Moreover, optimization of BHJ layers thicknesses is crucial in obtaining a high-performance tandem cell. To access in detail the balanced optical absorption and current matching, the BHJ layer thicknesses of the front and rear subcells must be optimized. Our tandem cell is limited by the photocurrent of the front subcell; thus, we carried out more optimization to determine the best current matching. In a tandem cell with identical or different BHJ layers, the number of absorbed photons from the incident solar energy,[40] charge carrier transport, as well as bimolecular recombination of charge carriers[41] must be optimized to match the photocurrents between the front and rear subcells. Low charge carrier mobilities and unbalanced electron/hole mobilities in organic solar cells[42,43] are characteristics of organic solar cells that make it complicated to match current densities between those subcells. Thus, a series of tandem cells was carefully designed to examine the effect of rear subcell thickness on the performance of the devices. The PSBTBT:PC_{70}BM BHJ layer thicknesses were varied from 90 to 130 nm. We set the front subcell BHJ layer thickness at 80 nm to match the current between those subcells as well as to keep adequate absorption and photocurrent in the rear subcell.

In order to check the reproducibility of our results, 173 tandem cells were fabricated and measured using optimized front and rear active layer thicknesses. Histograms of the photovoltaic parameters are shown in Figure 5. As can be seen from the results, these tandem cells are highly reproducible.

Figure 6 exhibits the $J-V$ curves of various sets of tandem cells with different PSBTBT:PC_{70}BM BHJ layer thicknesses (90−130 nm). The extracted photovoltaic parameters obtained from $J-V$ curves are summarized in Table 4. Table S5 (Supporting Information) summarizes the R_s and R_{sh} for all fabricated tandem cells with different rear subcell thicknesses. In these current-matching experiments, we observed that the

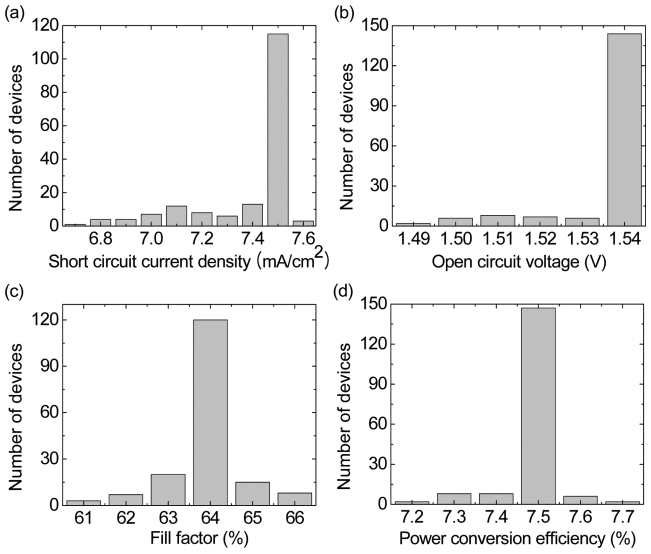

Figure 5. Histogram of tandem cell parameters measured for 173 separate glass/ITO/TiO_2/PBDTTPD:$PC_{61}BM$/pH-neutral PEDOT:PSS/LZO/PSBTBT:$PC_{70}BM$/MoO_3/Ag. J_{sc} (a), V_{oc} (b), FF (c), and PCE (d).

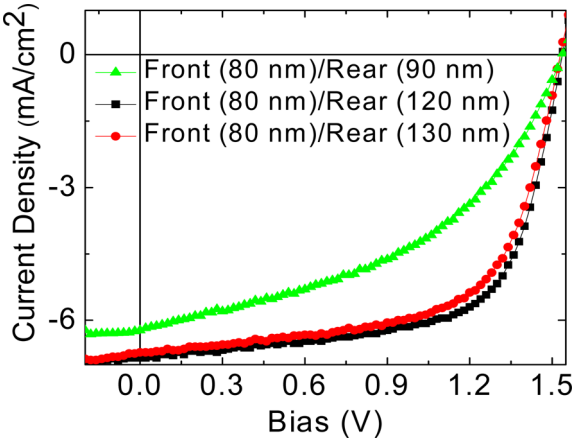

Figure 6. $J-V$ curves of tandem cells with various thicknesses of rear subcells.

Table 4. Device Performance of Organic Tandem Cells with Different Subcells Thicknesses

active layer thickness (front/rear) (nm)	J_{sc} (mA/cm^2)	V_{oc} (V)	FF (%)	PCE (%)
80/120	6.85 ± 0.1	1.54 ± 0.01	64.13 ± 0.11	6.86 ± 0.12
80/130	6.75 ± 0.1	1.54 ± 0.01	62.73 ± 0.05	6.50 ± 0.06
80/90	6.23 ± 0.1	1.54 ± 0.01	45.06 ± 0.06	4.32 ± 0.10

prepared tandem cells exhibit V_{oc}'s of about 1.54 V, which is the ideal summation value of the V_{oc}'s for the two subcells. From Table 4, the J_{sc} and FF change with various PSBTBT:$PC_{70}BM$ BHJ layer thicknesses.

As the PSBTBT:$PC_{70}BM$ BHJ thickness increases to 120 nm, the tandem cell still performs best when there is a slight increase in FF. Despite a small decrease in FF, one sees a decrease in J_{sc} to 6.85 mA/cm^2, yielding a considerable decrease in PCE, where PCE drops from 7.53% to 6.86%. Similarly, as the thickness of PSBTBT:$PC_{70}BM$ BHJ layer further increases, the tandem cell plummeted in both J_{sc} and FF. In the case for 130 nm thickness of the PSBTBT:$PC_{70}BM$ BHJ layer, the J_{sc} is 6.85 mA/cm^2, FF = 62.73%, and 6.50% PCE. Drastically reduced photovoltaic performance can be seen in the cell with 90 nm BHJ layer thickness. In this case, the J_{sc} and FF experience the biggest drop to values of 6.23 mA/cm^2 and 45.06% respectively, along with 4.32% PCE.

Since ICL has many functions, we extended our study with different ICLs. Table 5 summarizes the $J-V$ characteristics of a tandem solar cell with five different ICLs under 100 mW/cm^2 AM1.5G illumination. Table S6 (Supporting Information) collects the R_s and R_{sh} for all tandem cells with different concepts of ICLs. It is again worth mentioning that ICL should efficiently collect electrons from one cell and holes from another and act as an efficient recombination zone for them, free of potential loss.[44,45] On the basis of the characterization of front and rear single-junction solar cells, tandem solar cells with molybdenum oxide/graphene (MoO_3/G), pH-neutral PEDOT:PSS/polyethylenimine ethoxylated (PEIE), molybdenum oxide/aluminum/zinc oxide (MoO_3/Al/ZnO), Rhodamine B/gold (RhB/Au), and RhB ICLs were characterized. As shown in Figure 7a, the device performance of the tandem solar cells

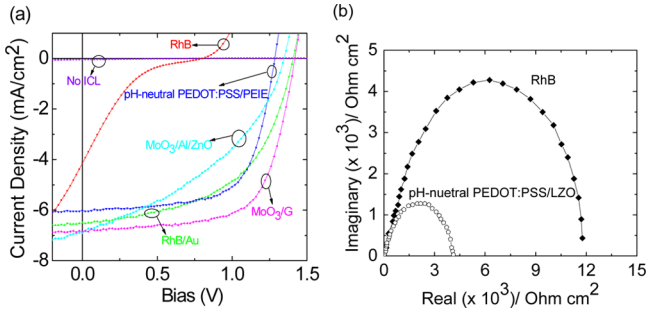

Figure 7. (a) $J-V$ curves of tandem cells with different ICLs under illumination. (b) Impedance spectra of tandem cells with RhB and pH-neutral PEDOT:PSS/LZO ICLs.

changes significantly when ICL varies. This indicates that in the tandem cell the ICL plays a critical role in the charge recombination process. The tandem cell without ICL demonstrated a V_{oc} of 0.13 V, a J_{sc} of 3.71 mA/cm^2, a FF of

Table 5. Device Performance of Organic Tandem Cells with Different Interconnecting Layers

interconnecting layer	J_{sc} (mA/cm^2)	V_{oc} (V)	FF (%)	PCE (%)
MoO_3/G	6.85 ± 0.11	1.42 ± 0.02	65.00 ± 0.02	6.41 ± 0.02
pH-neutral PEDOT:PSS/PEIE	6.03 ± 0.06	1.28 ± 0.01	66.13 ± 0.11	5.10 ± 0.11
MoO_3/Al/ZnO	6.90 ± 0.02	1.34 ± 0.01	39.91 ± 0.10	3.69 ± 0.07
RhB/Au	6.50 ± 0.10	1.40 ± 0.01	54.00 ± 0.12	4.91 ± 0.02
RhB	4.14 ± 0.10	0.82 ± 0.02	11.94 ± 0.12	0.39 ± 0.10
no ICL	3.71 ± 0.13	0.13 ± 0.01	0.20 ± 0.01	0.10 ± 0.11

dx.doi.org/10.1021/am5029318 | ACS Appl. Mater. Interfaces 2014, 6, 13079−13087

0.20%, and a PCE of 0.10%. The reduced photovoltaic performance of the tandem cell without an ICL suggests that the front and rear subcells are not electrically connected in series. The tandem cell fabricated with a MoO_3/Al/ZnO ICL coated on the front subcell led to a remarkable decrease in the V_{oc} from 1.54 to 1.34 V, yielding in an incredible PCE decrease from 7.53% to 3.69%. The V_{oc} for the tandem solar cell with a MoO_3/Al/ZnO ICL is 87% of the sum of the V_{oc} of the individual cells. In contrast, the tandem cell with MoO_3/G ICL shows a smaller value for V_{oc} (1.42 V), J_{sc} (6.85 mA/cm^2), and PCE (6.41%). The huge difference in the performance between tandem cells with pH-neutral PEDOT:PSS/LZO and MoO_3/G ICLs seems to be due to the accumulation of charges (holes within the MoO_3 layer and electrons within the G layer) as a result of the poor recombination rate at the interface of MoO_3 and G layers. This led to the decrease in both the current density through the whole device (J_{sc}) and the built-in potentials (V_{oc}). The tandem cell fabricated with pH-neutral PEDOT:PSS/PEIE ICL demonstrated a comparable tendency. Interestingly, the $J-V$ characteristics of the tandem cell incorporating RhB ICL have a dominant S-shaped kink curve with a high R_s of 862 Ω cm^2 giving a very low FF of 11.94%. The S-shaped kink curve corresponds to a considerable energy barrier for both charge extraction and injection processes. This energy barrier to charge carrier recombination results in accumulation of charge carriers, blocks charge extraction, and should be recombine within the active layers or near the interfaces of active layer/ICL, which causes V_{oc} losses; subsequently, increases in R_s result in a rather bad FF of 11.94%.[46,47] The S-shaped kink curve has been eliminated with the incorporation of an Au layer in conjunction with the RhB layer, which in this case yielded an increase in the FF to 54.00% and a decrease in the R_s to 116 Ω cm^2. This observation demonstrates that the RhB/Au ICL can provide an efficient recombination zone for holes and electrons generated from the front and rear subcells, respectively, due to the formation of improved Ohmic contacts. The increase in the PCE from 0.39% to 4.91% was obtained after the introduction of RhB/Au ICL in the tandem cell.

To further scrutinize the photovoltaic parameters of tandem cell with different ICLs, we carried out impedance spectroscopy measurements of the tandem cells with RhB and pH-neutral PEDOT:PSS/LZO ICLs. Impedance spectroscopy is a powerful method to not only characterize material properties but also to understand device operation as well as the stability of one particular system.[48−50]

Figure 7b depicts the typical complex impedance plan spectra of the tandem cells with different ICLs measured in the dark at zero bias. Figure 7b demonstrates the imaginary resistance over the real resistance, and there are two semicircles that can be found, which enables examination of the internal resistance of the ICLs. The distinctive feature in the complex plan is a combination of two semicircles that can be seen at low and high frequencies. The two semicircles are obviously seen with different diameters (the tandem cell using pH-neutral PEDOT:PSS/LZO ICL is smaller compared to the one with RhB ICL). We attribute this phenomenon to the charge extraction and injection resistance associated with the electron and hole recombination process in the pH-neutral PEDOT:PSS/LZO ICL. Moreover, the resistance of the tandem cell integrated with pH-neutral PEDOT:PSS/LZO ICL is smaller (1 Ω mm^2) than that of the tandem cell with RhB ICL (6.3 Ω mm^2). Thus, one could easily see that pH-neutral PEDOT:PSS/LZO ICL improved the tandem cell performance due to its less resistive ICL, which electrically connects the front and rear subcells.

3. CONCLUSIONS

In conclusion, we have demonstrated that high and low band gap polymers successfully fabricate the solution-processed inverted tandem solar cell. The tandem cells featuring a stack of polymeric/metal oxide ICL exhibit a PCE of 7.53% and a V_{oc} of 1.54 V. The nature of the ICLs has a strong influence on the output characteristics of the tandem cells. We studied various ICLs and demonstrated that the pH-neutral PEDOT:PSS/LZO stack possesses the appropriate carrier density and energy-level alignment to efficiently connect those two subcells. The advances presented here provide pathways for the design of an effective ICL in a solution-processed tandem cell.

4. EXPERIMENTAL SECTION

4.1. Materials. We purchased pH-neutral PEDOT:PSS from Sigma-Aldrich (Orgacon N-1005, 739324, pH 7, viscosity 3.6, solid content 1.2%). A low band gap polymer, PSBTBT, was supplied by Solarmer. A high band gap polymer, PBDTTPD, with an average molecular weight of 10 000−50 000 along with PDI ≤ 3.0, fullerenes ($PC_{61}BM$, and $PC_{70}BM$), MoO_3, PEIE, and titanium(IV) isopropoxide were obtained from Sigma-Aldrich. All materials were used without further purification.

4.2. Solution Preparation. LZO solution preparation has been published elsewhere.[50] The preparation of TiO_2 solution was completed according to a previously published article,[51] where titanium(IV) isopropoxide was used as precursor.

4.3. Device Fabrication. *Single Junction Fabrication (Front Subcell).* We cleaned ITO-patterned glass substrate in sequential ultrasonic baths in detergent, water, acetone, and 2-propanol, followed by 15 min UV−ozone treatment. TiO_2 was spun-cast at 1000 rpm (1 min) for 20 nm and baked at 100 °C for 10 min. Then the BHJ layer was spin-coated on the TiO_2 layer. The active layer was spun-cast at 700 rpm/1 min and baked at 115 °C for 10 min from solutions of 1:1.5 (wt/wt) PBDTTPD:$PC_{61}BM$ in chlorobenzene, which had been dissolved overnight. A total solution concentration of 20 mg mL^{-1} was used for the PBDTTPD:$PC_{61}BM$ device to produce an active layer thickness of 80 nm. Fifteen nanometers of pH-neutral PEDOT:PSS was spin-coated at 4000 rpm for 1 min and baked at 100 °C for 5 min, followed by 100 nm of Al, which was thermally evaporated under vacuum (<10^{-7} Torr) to provide the anode electrode, with a device area of 0.04 cm^2.

Single-Junction Fabrication (Rear Subcell). We cleaned ITO-patterned glass substrate in sequential ultrasonic baths using detergent, water, acetone, and 2propanol, followed by 15 min UV−ozone treatment. Thirty nanometers of LZO was spin-coated at 4000 rpm for 1 min on the ITO substrates and baked at 120 °C for 5 min. Next, the 100 nm active layer was spun-cast on the LZO layer. The rear subcell active layer was spun-cast at 4500 rpm for 1 min from PSBTBT:$PC_{70}BM$ (1:1) in chloroform (10 mg of PSBTBT/1 mL of solvent) followed by thermal annealing at 150 °C for 5 min. After spin-casting the active layer, the samples are transferred into the evaporation chamber for depositing the MoO_3 (5 nm)/Ag (100 nm) electrode with a device area of about 0.04 cm^2.

Tandem Devices Fabrication. Prepatterned ITO-coated glass substrates were cleaned as mentioned above. TiO_2 was spin-cast onto the cleaned ITO substrate at 4000 rpm for 1 min and left for 1 h for hydrolysis process. Later, the 20 nm TiO_2 layer was baked on a hot plate at 100 °C for 10 min, and 80 nm PBDTTPD:$PC_{61}BM$ for the front subcell was spin-cast at 700 rpm for 1 min. The PBDTTPD:$PC_{61}BM$ was then baked at 115 °C for 10 min. Following the front BHJ layer deposit, a 15 nm layer of pH-neutral PEDOT:PSS was spin-cast at 4000 rpm for 1 min and baked for 5 min at 100 °C on top to form the first ICL (Figure S3, Supporting Information). Prior to the deposition, the pH-neutral PEDOT:PSS was mixed with PTE

(pH-neutral) in order to get better wettability. The LZO layer was then spin-cast at 4000 rpm for 1 min and annealed at 120 °C for 5 min to complete the ICL (30 nm). Afterward, the rear subcell BHJ layer was spin-cast; the thickness was controlled by the spin-coating speed. The 100 nm PSBTBT:$PC_{70}BM$ was annealed at 150 °C for 5 min. Finally, the sample was transferred into the evaporation chamber for depositing 5 nm of MoO_3 followed by 100 nm of Ag as the top electrode; the device area was 0.04 cm^2.

4.4. Device Characterization. For tandem solar cells, the layers comprising TiO_2/PBDTTPD:$PC_{61}BM$/pH-neutral PEDOT:PSS/LZO/PSBTBT:$PC_{70}BM$ were electrically isolated using toluene and methanol along the perimeter defined by the top electrode to avoid the fringing effects and prevent overestimation of the photocurrent generated by the tandem cell. During the measurements and stability tests, a shadow mask (0.04 cm^2) with a single aperture was placed onto the tandem solar cells in order to define its photoactive area, and the device was illuminated at an intensity of 100 mW/cm^2 from a 1 kW solar simulator with an AM 1.5G filter in air. The light intensity is calibrated by a certified Oriel reference cell (91150 V). The current density−voltage (J−V) characteristics were recorded with a Keithley 2410 source meter. The external EQE measurements were performed using an EQE system (model 74000) obtained from Newport Oriel Instruments USA, and a HAMAMATSU calibrated silicon cell photodiode was used as a reference diode. The wavelength was controlled with a monochromator to be 300−900 nm.

Optical Simulation. We used our optical and electrical simulation tools for tandem polymer solar cell based on the transfer matrix formalism.[49] These tools determine the current density and power conversion efficiency based on a few factors, such as light transmission, reflection, absorption charge carrier transport including bimolecular recombination, exciton generation, dissociation probability, decay rate, dielectric constant, density of state, and carrier mobility.

■ ASSOCIATED CONTENT

Supporting Information

Transmittance, refractive index, extinction coefficient, and additional data. This material is available free of charge via the Internet at http://pubs.acs.org

■ AUTHOR INFORMATION

Corresponding Author

*Fax: +82 2 961 9154. Tel: +82 2 961 0607. E-mail: jjang@khu.ac.kr.

Notes

The authors declare no competing financial interest.

■ ACKNOWLEDGMENTS

This work was supported by CAPES-PNPD Project No. 3076/2010 and the Human Resources Development program (No. 20134010200490) of the Korea Institute of Energy Technology Evaluation and Planning (KETEP) grant funded by the Korea government Ministry of Trade, Industry and Energy.

■ REFERENCES

(1) Kim, J. Y.; Lee, K.; Coates, N. E.; Moses, D.; Nquyen, T. Q. Efficient Tandem Polymer Solar Cells Fabricated by All-Solution Processing. *Science* **2007**, *317*, 222−225.

(2) Dennler, G.; Scharber, M. C.; Ameri, T.; Denk, P.; Forberich, K.; Waldauf, C.; Brabec, C. J. Design Rules for Donors in Bulk-Heterojunction Tandem Solar Cells—Towards 15% Energy-Conversion Efficiency. *Adv. Mater.* **2008**, *20*, 579−583.

(3) Wang, X.; Koleilat, G. I.; Tang, J.; Liu, H.; Kramer, I. J.; Debnath, R.; Brzozowski, L.; Barkhouse, D. A. R.; Levina, L.; Hoogland, S.; Sargent, E. H. Tandem Colloidal Quantum Dot Solar Cells Employing a Graded Recombination Layer. *Nat. Photonics* **2011**, *5*, 480−484.

(4) Tung, V. C.; Kim, J.; Cote, L. J.; Huang, J. Sticky Interconnect for Solution-Processed Tandem Solar Cells. *J. Am. Chem. Soc.* **2011**, *133*, 9262−9265.

(5) Choi, J. J.; Wenger, W. N.; Hoffman, R. S.; Lim, Y. F.; Luria, J.; Jasieniak, J.; Marohn, J. A.; Hanrath, T. Solution-Processed Nanocrystal Quantum Dot Tandem Solar Cells. *Adv. Mater.* **2011**, *23*, 3144−3148.

(6) Yang, J.; Zhu, R.; Hong, Z.; He, Y.; Kumar, A.; Li, Y.; Yang, Y. A Robust Inter-Connecting Layer for Achieving High Performance Tandem Polymer Solar Cells. *Adv. Mater.* **2011**, *23*, 3465−3470.

(7) Gilot, J.; Wienk, M. M.; Janssen, R. A. J. Optimizing Polymer Tandem Solar Cells. *Adv. Energy Mater.* **2010**, *22*, E67−E71.

(8) Gilot, J.; Wienk, M. M.; Janssen, R. A. J. Measuring the External Quantum Efficiency of Two-Terminal Polymer Tandem Solar Cells. *Adv. Funct. Mater.* **2010**, *20*, 3904−3911.

(9) Gevaerts, V. S.; Furlan, A.; Wienk, M. M.; Turbiez, M.; Janssen, R. A. J. Solution Processed Polymer Tandem Solar Cell Using Efficient Small and Wide Bandgap Polymer:Fullerene Blends. *Adv. Mater.* **2012**, *24*, 2130−2134.

(10) Dou, L.; You, J.; Yang, J.; Chen, C.-C.; He, Y.; Murase, S.; Moriarty, T.; Emery, K.; Li, G.; Yang, Y. Tandem Polymer Solar Cells Featuring a Spectrally Matched Low-Bandgap Polymer. *Nat. Photonics* **2012**, *6*, 180−185.

(11) Riede, M.; Uhrich, C.; Widmer, J.; Timmreck, R.; Wynands, D.; Schwartz, G.; Gnehr, W. M.; Hildebrandt, D.; Weiss, A.; Hwang, J.; Sundarraj, S.; Erk, P.; Pfeiffer, M.; Leo, K. Efficient Organic Tandem Solar Cells Based on Small Molecules. *Adv. Funct. Mater.* **2011**, *21*, 3019−3028.

(12) Mishra, A.; Bauerle, P. Small Molecule Organic Semiconductors on the Move: Promises for Future Solar Energy Technology. *Angew. Chem., Int. Ed.* **2012**, *51*, 2020−2067.

(13) Tan, Z.; Zhang, W.; Zhang, Z.; Qian, D.; Huang, Y.; Hou, J.; Li, Y. High-Performance Inverted Polymer Solar Cells with Solution-Processed Titanium Chelate as Electron-Collecting Layer on ITO Electrode. *Adv. Mater.* **2012**, *24*, 1476−1481.

(14) Nattestad, A.; Mozer, A. J.; Fischer, M. K. R.; Cheng, Y. B.; Mishra, A.; Bauerle, P.; Bach, U. Highly Efficient Photocathodes for Dye-Sensitized Tandem Solar Cells. *Nat. Mater.* **2010**, *9*, 31−35.

(15) Miao, Q.; Wu, L.; Cui, J.; Huang, M.; Ma, T. A New Type of Dye-Sensitized Solar Cell with a Multilayered Photoanode Prepared by a Film-Transfer Technique. *Adv. Mater.* **2011**, *23*, 2764−2768.

(16) Soderstrom, T.; Haug, F. J.; Daudrix, V. T.; Ballif, C. Flexible Micromorph Tandem a-Si/μc-Si Solar Cells. *J. Appl. Phys.* **2010**, *107*, 014507.

(17) Upping, J.; Bielawny, A.; Wehrspohn, R. B.; Beckers, T.; Carius, R.; Rau, U.; Fahr, S.; Rockstuhl, C.; Lederer, F.; Kroll, M.; Pertsch, T.; Steidl, L.; Zentel, R. Three-Dimensional Photonic Crystal Intermediate Reflectors for Enhanced Light-Trapping in Tandem Solar Cells. *Adv. Mater.* **2011**, *23*, 3896−3900.

(18) Jeong, W. S.; Lee, J. W.; Jung, S.; Yun, J. H.; Park, N. G. Evaluation of External Quantum Efficiency of a 12.35% Tandem Solar Cell Comprising Dye-Sensitized and CIGS Solar Cells. *Sol. Energy Mater. Sol. Cells* **2011**, *95*, 3419−3423.

(19) Wang, W. L.; Lin, H.; Zhang, J.; Li, X.; Yamada, A.; Konagai, M.; Li, J. B. Experimental and Simulation Analysis of the Dye Sensitized Solar Cell/Cu(In,Ga)Se_2 Tandem Structure. *Sol. Energy Mater. Sol. Cells* **2010**, *94*, 1753−1758.

(20) Barber, G. D.; Hoertz, P. G.; Lee, S. H. A.; Abrams, N. M.; Mikulca, J.; Mallouk, T. E.; Liska, P.; Zakeeruddin, S. M.; Gratzel, M.; Baillie, A. H.; Green, M. A. Utilization of Direct and Diffuse Sunlight in a Dye-Sensitized Solar Cell−Silicon Photovoltaic Hybrid Concentrator System. *J. Phys. Chem. Lett.* **2011**, *2*, 581−585.

(21) Hao, S.; Wu, J.; Sun, Z. A Hybrid Tandem Solar Cell Based on Hydrogenated Amorphous Silicon and Dye-Sensitized TiO_2 Film. *Thin Solid Films* **2012**, *520*, 2102−2105.

(22) Shao, S.; Zheng, K.; Pullerits, T.; Zhang, F. Enhanced Performance of Inverted Polymer Solar Cells by Using Poly(ethylene oxide)-Modified ZnO as an Electron Transport Layer. *ACS Appl. Mater. Interfaces* **2013**, *5*, 380.

(23) Shao, S.; Liu, J.; Bergqvist, J.; Shi, S.; Veit, C.; Xie, Z.; Zhang, F. n Situ Formation of MoO3 in PEDOT:PSS Matrix: A Facile Way To Produce a Smooth and Less Hygroscopic Hole Transport Layer for Highly Stable Polymer Bulk Heterojunction Solar Cells. *Adv. Energy Mater.* **2013**, *3*, 349.
(24) You, J.; Chen, C.-C.; Hong, Z.; Yoshimura, K.; Ohya, K.; Xu, R.; Ye, S.; Gao, J.; Li, G.; Yang, Y. 10.2% Power Conversion Efficiency Polymer Tandem Solar Cells Consisting of Two Identical Sub-Cells. *Adv. Mater.* **2013**, *25*, 3973−3978.
(25) Sista, S.; Park, M.-H.; Hong, Z.; Wu, Y.; Hou, J.; Kwan, W. L.; Li, G.; Yang, Y. Highly Efficient Tandem Polymer Photovoltaic Cells. *Adv. Mater.* **2010**, *22*, 380−383.
(26) Yusoff, A. R. B. M.; Lee, S. J.; Shneider, F. K.; da Silva, W. J.; Jang, J. High-Performance Semitransparent Tandem Solar Cell of 8.02% Conversion Efficiency with Solution-Processed Graphene Mesh and Laminated Ag Nanowire Top Electrodes. *Adv. Energy Mater.* DOI:10.1002/aenm.201301989.
(27) Liu, J.; Shao, S.; Fang, G.; Wang, J.; Meng, B.; Xie, Z.; Wang, L. High-Efficiency Inverted Tandem Polymer Solar Cells with Step-Al-Doped MoO_3 Interconnection Layer. *Sol. Energy Mater. Sol. Cells* **2014**, *120*, 744.
(28) www.heliatek.com/newscenter/latest_news/.
(29) You, J.; Dou, L.; Yoshimura, K.; Kato, T.; Ohya, K.; Moriarty, T.; Emery, K.; Chen, C.-C.; Gao, J.; Li, G.; Yang, Y. A Polymer Tandem Solar Cell with 10.6% Power Conversion Efficiency. *Nat. Commun.* **2012**, *4*, 1446.
(30) Li, W.; Furlan, A.; Hendriks, K. H.; Wienk, M. M.; Janssen, R. A. J. Efficient Tandem and Triple-Junction Polymer Solar Cells. *J. Am. Chem. Soc.* **2013**, *135*, 5529−5532.
(31) Yusoff, A. R. B. M.; Lee, S. J.; Kim, H. P.; Shneider, F. K.; da Silva, W. J.; Jang, J. 8.91% Power Conversion Efficiency for Polymer Tandem Solar Cells. *Adv. Funct. Mater.* **2014**, *24*, 2240−2247.
(32) Gil, T. H.; May, C.; Scholz, S.; Franke, S.; Toerker, M.; Lakner, H.; Leo, K.; Kellerc, S. Origin of Damages in OLED from Al Top Electrode Deposition by DC Magnetron Sputtering. *Org. Electron.* **2011**, *11*, 322.
(33) Kim, D. H.; Kim, D. W.; Kim, K. S.; Kim, H. J.; Moon, J. S.; Hong, M. P.; Kim, B. S.; Shin, J. H.; Kim, Y. M.; Song, K. K.; Shin, S. S. Effects of Plasma Process Induced Damages on Organic Gate Dielectrics of Organic Thin-Film Transistors. *Jpn. J. Appl. Phys.* **2008**, *47*, 5672−5675.
(34) Zou, Y.; Najari, A.; Beerouard, P.; Bearupre, S.; Aich, B. R.; Tao, Y.; Leclerc, M. A Thieno[3,4-*c*]pyrrole-4,6-dione-Based Copolymer for Efficient Solar Cells. *J. Am. Chem. Soc.* **2010**, *132*, 5330−5331.
(35) Hou, J.; Chen, H.-Y.; Zhang, S.; Li, G.; Yang, Y. Synthesis, Characterization, and Photovoltaic Properties of a Low Band Gap Polymer Based on Silole-Containing Polythiophenes and 2,1,3-Benzothiadiazole. *J. Am. Chem. Soc.* **2008**, *130*, 16144−16145.
(36) Shneider, F. K.; da Silva, W. J.; Yusoff, A. R. B. M. Manuscript under review.
(37) Hadipour, A.; de Boer, B.; Blom, P. W. M. Device Operation of Organic Tandem Solar Cells. *Org. Electron.* **2008**, *9*, 617−624.
(38) Peters, C. H.; Sachs-Quitana, I. T.; Kastrop, J. P.; Beaupre, S.; Leclerc, M.; McGehee, M. D. High Efficiency Polymer Solar Cells with Long Operating Lifetimes. *Adv. Energy Mater.* **2011**, *1*, 491−494.
(39) Dennler, G.; Forberich, K.; Ameri, T.; Waldauf, C.; Denk, P.; Brabec, C. J. Design of Efficient Organic Tandem Cells: On the Interplay between Molecular Absorption and Layer Sequence. *J. Appl. Phys.* **2007**, *102*, 123109.
(40) Pivrikas, A.; Sariciftci, N. S.; Juska, G.; Osterbacka, R. A Review of Charge Transport and Recombination in Polymer/Fullerene Organic Solar Cells. *Prog. Photovoltaics* **2007**, *15*, 677−696.
(41) Lenes, M.; Koster, L. J. A.; Mihailetchi, V. D.; Blom, P. W. M. Thickness Dependence of the Efficiency of Polymer:Fullerene Bulk Heterojunction Solar Cells. *Appl. Phys. Lett.* **2006**, *88*, 243502.
(42) Koster, L. J. A.; Mihailetchi, V. D.; Blom, P. W. M. Bimolecular Recombination in Polymer/Fullerene Bulk Heterojunction Solar Cells. *Appl. Phys. Lett.* **2006**, *88*, 052104.
(43) Yuan, Y.; Huang, J.; Li, G. Organic Solar Cell—Intermediate Layers in Tandem Organic Solar Cells. *Green* **2011**, *1*, 65.
(44) Sista, S.; Hong, Z.; Chen, L. M.; Yang, Y. Tandem Polymer Photovoltaic Cells—Current Status, Challenges and Future Outlook. *Energy Environ. Sci.* **2011**, *4*, 1606−1620.
(45) Yakimov, A.; Forrest, S. R. High Photovoltage Multiple-Heterojunction Organic Solar Cells Incorporating Interfacial Metallic Nanoclusters. *Appl. Phys. Lett.* **2002**, *80*, 1667.
(46) Kumar, A.; Sista, S.; Yang, Y. Dipole Induced Anomalous S-Shape I−V Curves in Polymer Solar Cells. *J. Appl. Phys.* **2009**, *105*, 094512.
(47) Glatthaar, M.; Riede, M.; Keegan, N.; Sylvester-Hvid, K.; Zimmermann, B.; Niggemann, M.; Hinsch, A.; Gombert, A. Efficiency Limiting Factors of Organic Bulk Heterojunction Solar Cells Identified by Electrical Impedance Spectroscopy. *Sol. Energy Mater. Sol. Cells* **2007**, *91*, 390−393.
(48) Glatthaar, M.; Mingirulli, M.; Zimmermann, B.; Ziegler, T.; Kern, R.; Niggemann, M.; Hinsch, A.; Gombert, A. Impedance Spectroscopy on Organic Bulk-Heterojunction Solar Cells. *Phys. Status Solidi A* **2005**, *202*, R125−R127.
(49) Knipper, M.; Parisi, J.; Coakley, K.; Waldauf, C.; Brabec, C. J.; Dyakonov, V. Impedance Spectroscopy on Polymer−Fullerene Solar Cells. *Z. Naturforsch. A* **2007**, *62*, 490−494.
(50) Lee, S. J.; Kim, H. P.; Yusoff, A. R. B. M.; Jang, J. Organic Photovoltaic with PEDOT:PSS and V_2O_5 Mixture as Hole Transport Layer. *Sol. Energy Mater. Sol. Cells* **2013**, *120*, 238−243.
(51) Hadipour, A.; Muller, R.; Heremans, P. Room Temperature Solution-Processed Electron Transport Layer for Organic Solar Cells. *Org. Electron.* **2013**, *14*, 2379−2386.